J IRAN CHEM SOC (2017) 14:2229–2238
DOI 10.1007/s13738-017-1159-0

ORIGINAL PAPER

Electrochemical synthesis of nickel–cobalt oxide nanoparticles on the glassy carbon electrode and its application for the voltammetric determination of 4-nitrophenol

Karim Asadpour-Zeynali[1] · Elnaz Delnavaz[1]

Received: 3 February 2017 / Accepted: 13 June 2017 / Published online: 19 June 2017

Abstract In this article, a new voltammetric sensor for determination of 4-nitrophenol (4-NP) based on nickel–cobalt oxide nanoparticle (Ni–Co_{OX} NPs)-modified glassy carbon electrode (GCE) was presented. The nickel–cobalt nanoparticles (Ni–Co NPs) were firstly electrodeposited on the GCE by repetitive potential cycling method, and then, the deposited NPs were converted to Ni–Co_{OX} NPs by sweeping the potential of the electrode from 0.0 to 0.6 V in 0.1 M NaOH solution. The obtained electrocatalyst (Ni–Co_{OX} NPs) was analysed via scanning electron microscopy and energy-dispersive X-ray spectroscopy. 4-Nitrophenol showed a well-defined reduction peak at about −733 mV at the Ni–Co_{OX} NPs/GCE in the phosphate buffer solution (pH 6.0). Compared with the bare GCE, the reduction peak current was clearly enhanced and the overpotential was significantly decreased at the Ni–Co_{OX} NPs/GCE. The diffusion coefficient (D) of 4-nitrophenol at the modified electrode was also determined utilizing chronoamperometry. The current response of the modified electrode was linear with the 4-NP concentration in the range from 7 to 682 μM, with a detection limit of 4.8 μM ($S/N = 3$), using differential pulse voltammetry.

✉ Karim Asadpour-Zeynali
asadpour@tabrizu.ac.irk; k.zeynali@gmail.com

[1] Department of Analytical Chemistry, Faculty of Chemistry, University of Tabriz, Tabriz 51666-16471, Iran

Graphical Abstract

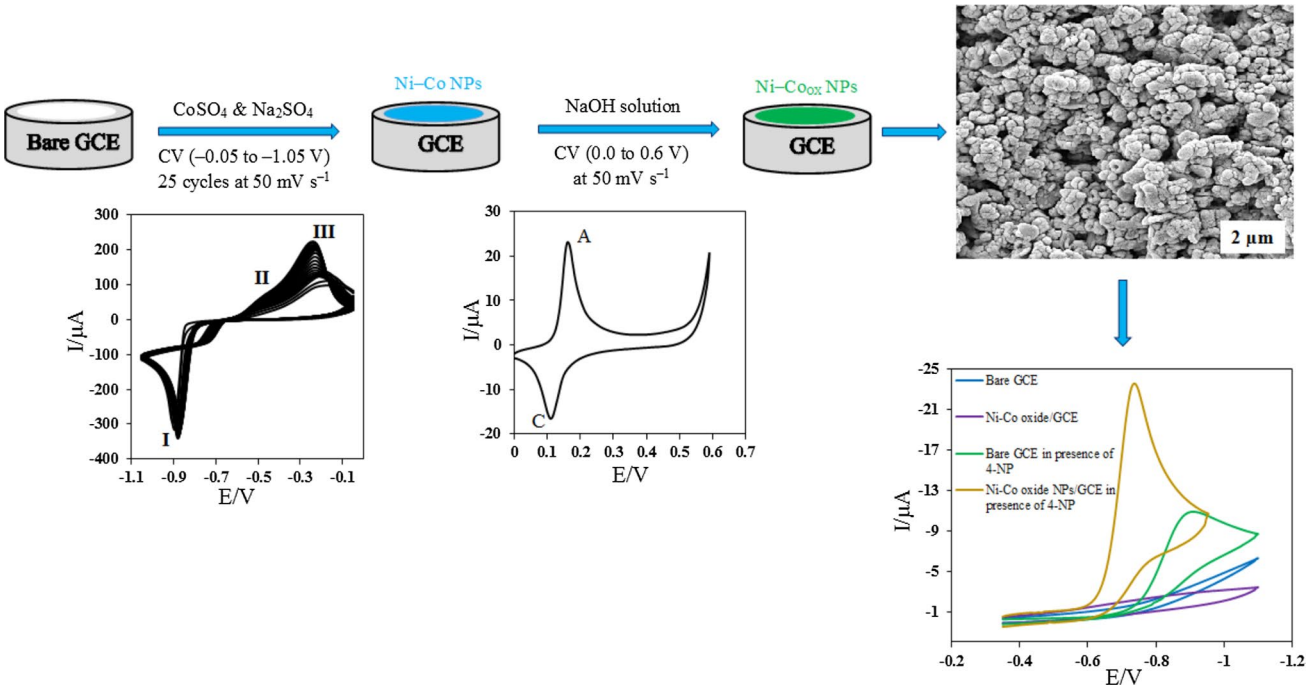

Keywords Differential pulse voltammetry · Modified glassy carbon electrode · Nickel–cobalt oxide nanoparticles · 4-Nitrophenol

Introduction

Phenolic compounds are recognized as the most serious pollutants because of their high toxicity on human and environment even in very low concentrations [1]. In addition, the degradation of these compounds is very difficult due to the presence of aromatic ring in their structures, and so they remain in the environment for a long period of time [2, 3]. 4-Nitrophenol (4-NP), one of the phenolic compounds, is extensively utilized in the synthesis of pesticides, dyes, darken leathers, insecticides, pharmaceutical compounds, and so on. Despite its wide applications, this compound is among the highly hazardous phenols to living beings due to its carcinogenic, mutagenic, and dermatological effects [5, 42]. 4-Nitrophenol is also known as an industrial pollutant and shows high solubility and stability in aquatic environments [4–7]. Thus, the development of efficient and simple analytical methods for the selective and sensitive determination of 4-NP is needed. Several techniques including high-performance liquid chromatography [8], UV–visible spectrophotometry [9], capillary electrophoresis [10], and fluorescence [11] have been reported for the determination of 4-NP in environmental samples. Most of these methods are relatively expensive, time-consuming, complicated, and require large amounts of organic solvents. Among them, electrochemical techniques based on modified electrodes offer an alternative way to detect 4-NP and have some advantages such as fast response, easy preparation, low cost, feasibility of miniaturization, high sensitivity, and selectivity [6]. Thus, various modified electrodes such as SWNT/GCE [1], MWNT-Nafion/GCE [12], reduced graphene oxide and molecularly imprinted polymer-modified GCE [13], and polyelectrolyte-functionalized graphene-modified GCE [14] have been developed to determine 4-NP. However, little attention has been paid to the electrocatalytic activity of metal and metal-oxide-modified electrodes in electrochemical reduction of 4-NP.

Numerous metal and metal oxide nanoparticles (NPs), including ZnO [15], Co_3O_4 [16], CuO [17], NiO [18], Cu [19], and Ni [20], have received a great interest in many fields. Among them, cobalt oxide and nickel oxide NPs are very attractive due to their unique properties such as large surface area, excellent conductivity, electrocatalytic and catalytic activities, low cost, abundant resource, and low toxicity [21–23]. Therefore, these metallic oxides and their bimetallic oxides have been successfully used for various applications, including sensors and biosensors. Recently, Noorbaksh et al. [24] made a sensitive electrochemical sensor based on cobalt oxide nanostructure-modified GCE for the determination of para-nitrophenol. Zhang et al. [25] presented a nanoenzymatic glucose sensor based on graphene oxide and electrospun NiO nanofibers. Cox and Pletcher [26] utilized the Co–Ni oxides as an efficient

electrocatalysts for the oxidation of ethanol to acetic acid. Among the several methods that have been developed for the fabrication of metal oxides, the electrochemical deposition has drawn remarkable attention between the researchers owing to its comparatively simpleness and cost-effectiveness over other methods. Moreover, the electrochemical methods prepared a uniform and thin film with high adhesion and special composition that can be easily controlled by changing the experimental parameters, such as current density, applied potential, solution composition and pH, number of potential scan [27].

In the present work, Ni–Co_{OX} NPs were electrodeposited on the surface of GCE by repetitive potential cycling method. The Ni–Co_{OX} NP-modified GCE exhibited high catalytic activity towards the reduction of 4-NP. Therefore, the prepared electrochemical sensor was successfully used for the determination of 4-NP in environmental water samples.

Experimental

Chemicals and reagents

$NiCl_2{\cdot}6H_2O$, $CoCl_2{\cdot}6H_2O$, KCl, NaOH, and 4-NP were obtained from Merck. The stock solution of 4-NP (0.5 mM) was prepared by dissolving an accurate amount of 4-NP in deionized water and then kept in a refrigerator [14]. The phosphate buffer solutions in the range of 4.0–11.0 (PBSs 0.1 M) were prepared from H_3PO_4, KH_2PO_4, and K_2HPO_4. Deionized water was from Ghazi Company (Tabriz, Iran). Before all experiments, the solutions were deoxygenated with pure nitrogen gas (99.999%) for 15 min.

Apparatus and software

All voltammetry measurements were taken with a Metrohm 757 VA processor at the room temperature (T = 298 K). The conventional three-electrode system consisted of a bare or a modified glassy carbon electrode serving as the working electrode (surface area of 0.0314 cm^{-2}), a platinum wire as the counter electrode, and a saturated calomel electrode (SCE) as the reference electrode (in saturated KCl). In order to determine the detection limit, the differential pulse voltammograms were recorded from −0.4 to −1.0 V and with following parameters: pulse time = 40 ms, pulse amplitude = 50 mV and scan rate = 50 mV s^{-1}. Surface morphology and chemical composition of the deposited nanoparticles were evaluated by scanning electron microscopy (SEM) at 10 kV on a MIRA3 TESCAN equipped with the energy-dispersive X-ray (EDX) analyser.

Preparation of the Ni–Co_{OX} NPs/GCE

Before modification, the GCE was polished with a 0.05-μm alumina suspension sequentially, rinsed with distilled water, then sonicated in ethanol and distilled water (1:1, v:v) for 10 min. The modified GCE was prepared under the following optimum conditions: First, the bimetallic Ni–Co NPs were electrochemically deposited on the GCE by potential cycling (25 cycles at 50 mV s^{-1}) between –0.05 and –1.05 V from 0.1 M KCl solution composed of 1:3 ratio of $NiCl_2{\cdot}6H_2O$ and $CoCl_2{\cdot}6H_2O$ (total concentration of two salts was equal to 20.0 mM). Then, the oxidization of deposited nanoparticles was processed by scanning potential between 0.0 and 0.6 V in 0.1 M NaOH solution at a scan rate of 50 mV s^{-1} until the stable voltammograms were obtained. When not in use, the prepared Ni–Co_{OX} NP-modified electrode was stored in 0.1 M NaOH solution.

Results and discussion

Electrodeposition of Ni–Co_{OX} NPs/GCE

Figure 1 reveals the consecutive cyclic voltammograms (CVs) of the electrodeposition of the Ni–Co NPs on the electrode surface in the preparation solution. As shown, a large cathodic peak was appeared at –0.88 V (peak I), which can be ascribed to the reduction of Ni^{2+} and Co^{2+} on the GCE to form Ni–Co NPs. The two anodic peaks at −0.49 V (peak II) and −0.25 V (peak III) were attributed

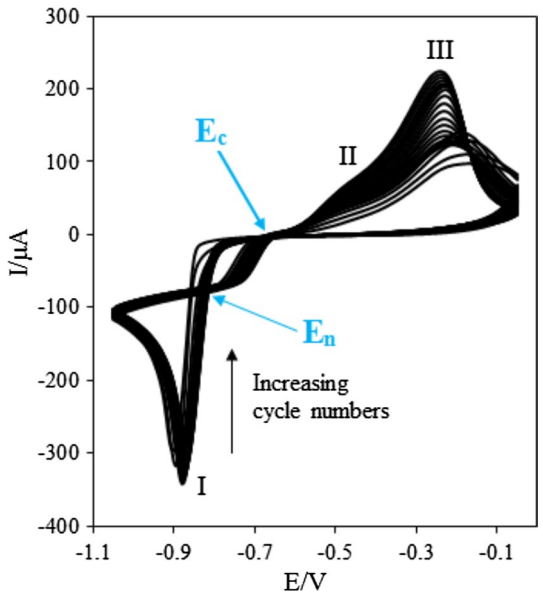

Fig. 1 CVs of GCE in 0.1 M KCl + 0.015 M $CoCl_2$ + 0.005 M $NiCl_2$ at 50 mV s^{-1}

to the oxidation of the deposited Ni–Co NPs from the electrode surface [22, 28, 29]. The cathodic current decreased with the proceeding of potential scan number, demonstrating that Ni^{2+} and Co^{2+} have been successfully reduced on the electrode surface. Electrochemical deposition of metal ions on a foreign substrate (e.g. GCE) requires more negative potential than that was required to reduce on the electrode made of the metal. Therefore, on the forward scan the deposition of cobalt and nickel on GCE started at more negative potentials than the redox potentials of each ion. However, on the reverse scan the deposition was happened on the substrate that already has been covered with the metal deposited, and so continued until the redox potentials were reached. Owing to the difference in deposition potentials of metal ions on the forward and reversed scan, a crossover was appeared, which was determined as the nucleation overpotential (E_n). The second crossover was appeared at less cathodic potentials (E_c), which was due to the difference between the deposition and dissolution potentials of metal ions [30–32].

It can be seen that just a reduction peak was appeared on the forward sweep towards the negative potentials. Therefore, independent electrodepositions of nickel and cobalt were investigated from individual solutions that each contains the same concentration of Ni^{2+} and Co^{2+} (0.01 M) and the 25th CVs of the GCE recorded. As shown in Fig. 2, the reduction potentials of Ni^{2+} and Co^{2+} from individual solutions were very close to each other, which means that the Ni–Co NPs were co-deposited on the GCE at the same potential from an aqueous solution [22, 28, 29].

Figure 3 shows a typical CV of the modified GCE with Ni–Co NPs in 0.1 M NaOH solution. According to the previous observations, the anodic peak (peak A) can be expressed by the following reactions [29, 33–38]:

$$Ni(OH)_2 + OH^- \rightarrow NiOOH + H_2O + e \quad (1)$$

$$Co(OH)_2 + OH^- \rightarrow CoOOH + H_2O + e \quad (2)$$

During the forward sweep towards more positive potentials, CoOOH was further oxidized into CoO_2 and can be described with the following reaction [29, 33–38]:

$$CoOOH + OH^- \rightarrow CoO_2 + H_2O + e \quad (3)$$

Therefore, the Ni–Co NPs were converted to the Ni–Co_{OX} NPs by sweeping potential in the alkaline medium.

Surface characterization of the electrodeposited Ni–Co_{OX} NPs

The surface morphology of electrodeposited Ni–Co_{OX} NPs was evaluated by SEM technique, and the corresponding images are depicted in Fig. 4a–c. It can be seen that the

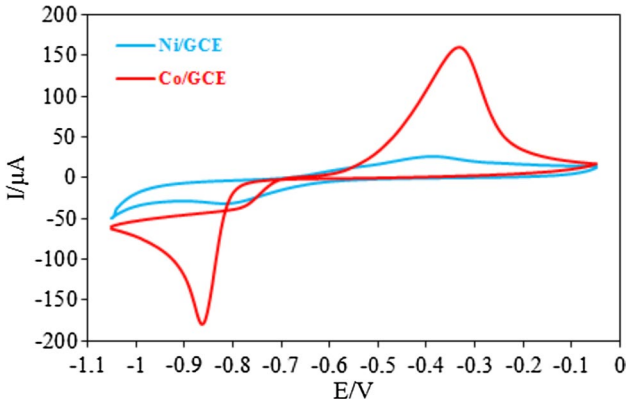

Fig. 2 25th CVs of GCE in 0.1 M KCl solutions containing of 0.01 M $CoCl_2$ and 0.01 M $NiCl_2$ at 50 mV s^{-1}

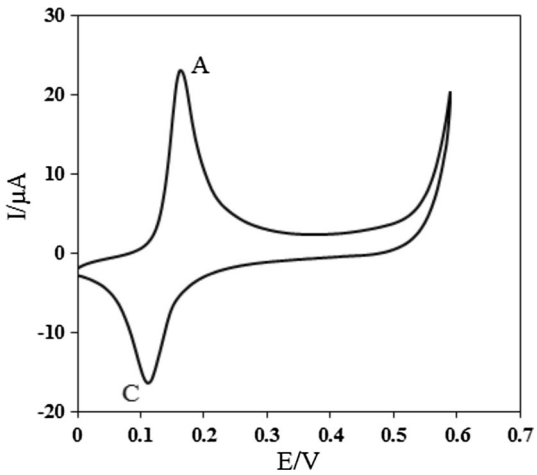

Fig. 3 CV of Ni–Co NPs/GCE in 0.1 M NaOH solution at of 50 mV s^{-1}

cauliflower-like particles with high density were distributed uniformly on the electrode surface. Also, the particles with average size less than 100 nm were observed on the image. The EDX patterns of the Ni–Co_{OX} NPs/GCE clearly confirmed the presence of the Ni and Co nanoparticles on the electrode surface (Fig. 4d).

Electrocatalytic reduction of 4-NP on the Ni–Co_{OX} NPs/GCE

The CVs of 0.5 mM, 4-NP at a bare GCE and Ni–Co_{OX} NP-modified electrode in the absence and presence of 4-NP in 0.1 M PBS (pH 6.0) are shown in Fig. 5. At the bare glassy carbon electrode, 4-NP showed an irreversible reduction peak at about −889 mV. But at the Ni–Co_{OX} NP-modified electrode, the reduction peak current was remarkably enhanced and the peak potential shifted

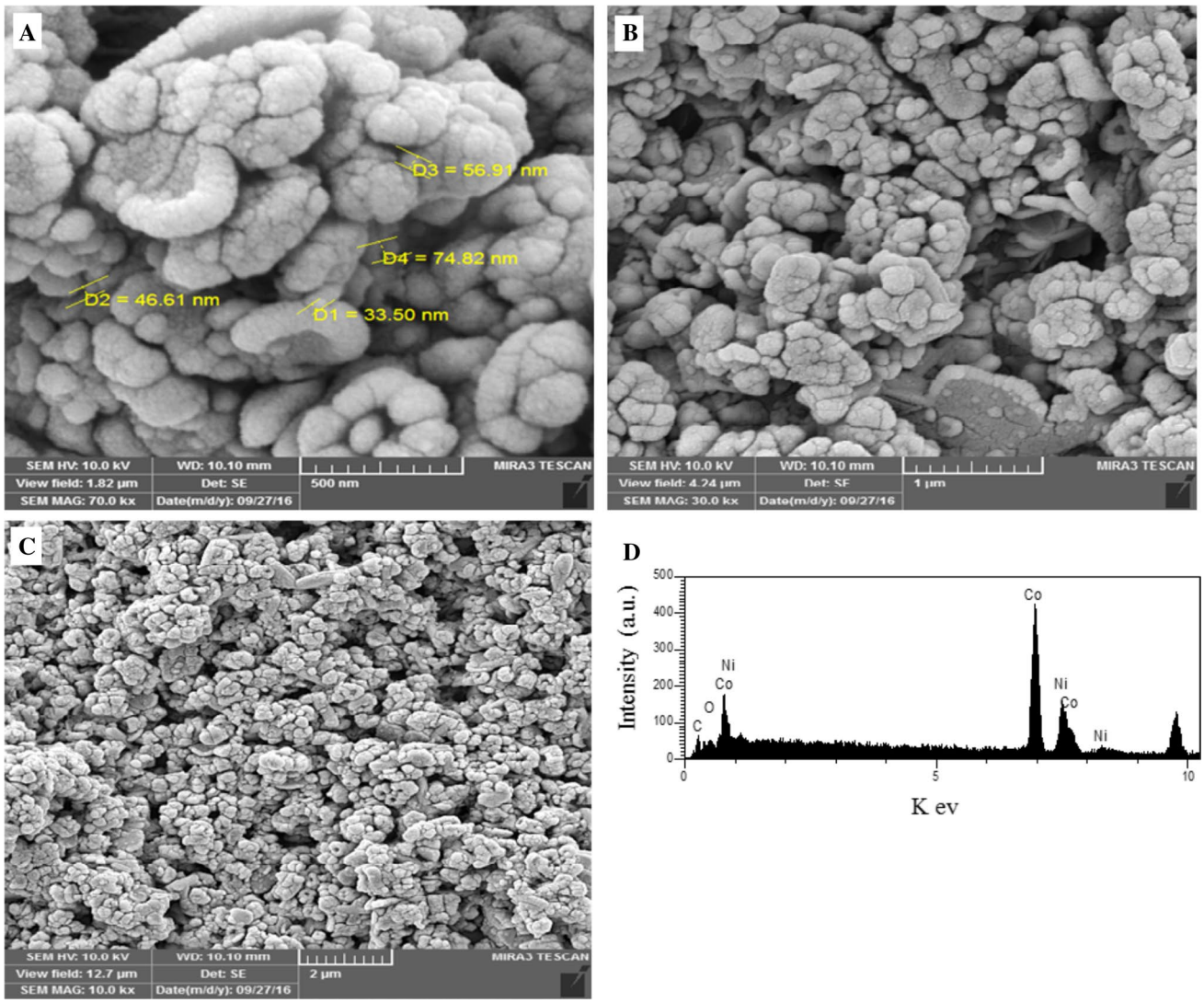

Fig. 4 SEM images of the Ni–Co_{OX} NPs/GCE with different magnifications (**a**–**c**). EDX patterns of Ni–Co_{OX} NPs/GCE (**d**)

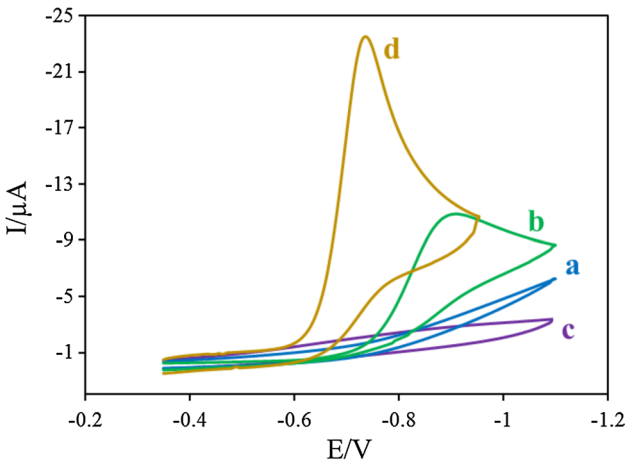

Fig. 5 CVs of the bare GCE in the absence (*a*) and presence (*b*) of 0.5 mM, 4-NP. *c* and *d* as *a* and *b* for the Ni–Co_{OX} NPs/GCE, in 0.1 M PBS (pH 6.0) at 50 mV s^{-1}

positively at about −733 mV. The marked increase in the peak current and decrease in the overpotential of 4-NP reduction at the modified electrode could be attributed to the high catalytic ability of Ni–Co_{OX} nanoparticles.

Effect of pH

The effect of pH on the electrocatalytic reduction of 4-NP at the Ni–Co_{OX} NPs/GCE was explored in the pH range of 11.0 to 4.0 by cyclic voltammetry. As shown in Fig. 6, the values of the reduction peak current and potential of 4-NP were dependent on the pH of the supporting electrolyte. The peak current progressively increased with decreasing of pH from 11.0 to 6.0 and then decreased from pH 6.0 to 4.0. Therefore, pH 6.0 was selected as the optimum pH for the subsequent electrochemical experiments, while the peak potential

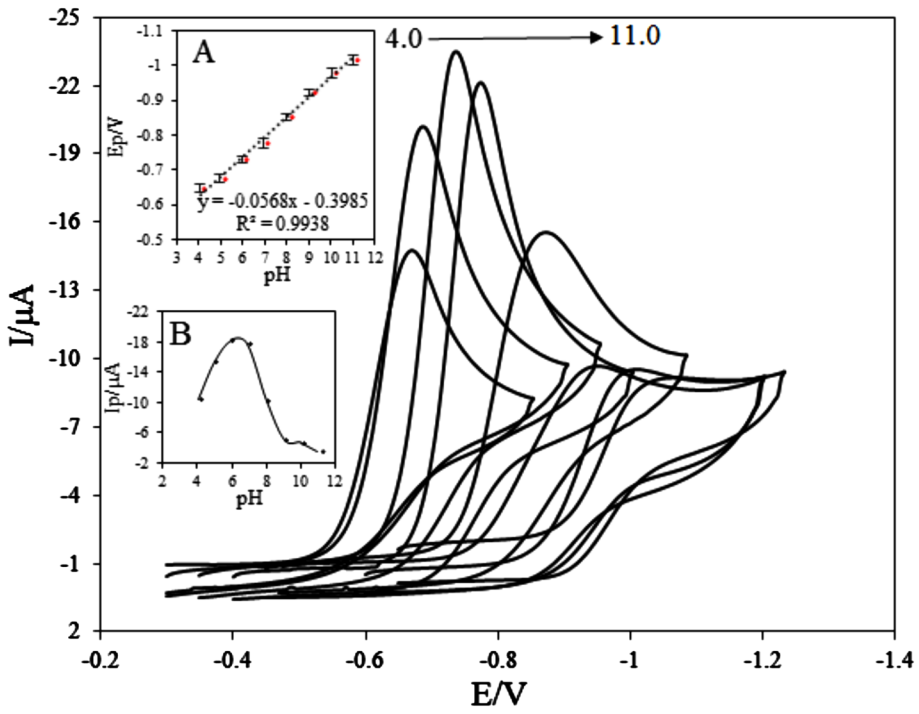

Fig. 6 CVs of 0.5 mM, 4-NP in the pH range of 4.0–11.0 in 0.1 M PBS at Ni–Co_{OX} NPs/GCE at 50 mV s^{-1}. *Inset a* and *b* represents the variation of the cathodic peak currents and the peak potentials versus pH values, respectively

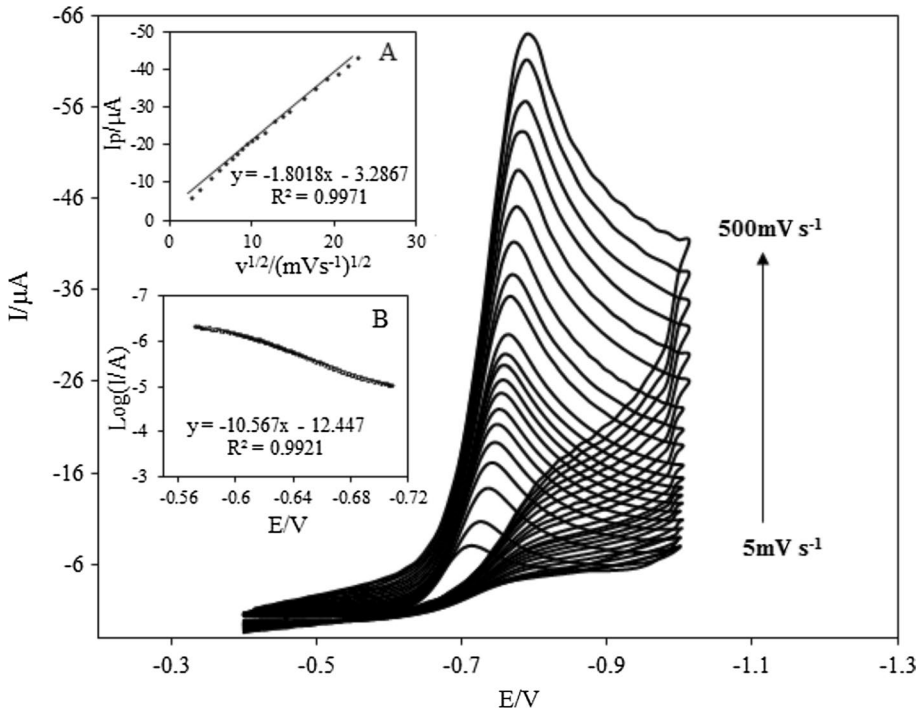

Fig. 7 CVs of the Ni–Co_{OX} NPs/GCE in the presence of 0.5 mM, 4-NP in 0.1 M PBS (pH 6.0) at scan rates of 5, 10, 20, 30, 40, 50, 60, 70, 80, 90, 100, 125, 150, 175, 200, 250, 300, 350, 400, 450, and 500 mV s^{-1}. *Inset a* the plot of peak currents versus square root of scan rates. *Inset b* Tafel plot obtained from current–potential curve in the presence of 0.5 mM 4-NP in 0.1 M PBS at 10 mV s^{-1}

values shifted to less negative potentials with decreasing of pH from 11.0 to 4.0 and obeyed from the following equation: E_{pc} (V) = −0.0568 pH − 0.3985. This slope demonstrated that equal number of protons and electrons was participated in the electrochemical reduction of 4-NP.

Effect of scan rate

The electrochemical behaviours of 4-NP at various scan rates (5–500 mV s^{-1}) were studied on the modified GCE by cyclic voltammetry in phosphate buffer solution (Fig. 7). As shown in Fig. 7a, the values of peak

currents were linearly proportional to the square root of scan rates, demonstrating that the reduction process of 4-NP at the Ni–Co_{OX} NPs/GCE was controlled by diffusion. The reduction peak potential shifted to more negative potentials with increasing the scan rate indicating a kinetic limitation in the reaction between the redox sites of Ni–Co_{OX} NPs and 4-NP (Fig. 7).

In order to calculate the kinetic parameters of 4-NP at the Ni–Co_{OX} NPs/GCE, the Tafel plot was drawn at a scan rate of 10 mV s^{-1} (Fig. 7b). According to the Butler–Volmer equation for a cathodic branch [39]:

$$\text{Log } I = \text{LogI}_0 + \frac{-\alpha n_\alpha F}{2.303RT}\eta \quad (4)$$

where α is the charge transfer coefficient of the electrochemical reaction, n_α is the number of electrons involved in the rate-determining step, I_0 is the exchange current density, R is the universal gas constant (8.314 J K^{-1} mol^{-1}), F is the Faraday constant (96,485 C mol^{-1}), T is the temperature (K), and η is the overpotential. The slope ($\alpha n_\alpha F/2.303RT$) of 10.567 V $decade^{-1}$ was observed, indicating that one electron was transferred in the rate-determining step and the value of α was calculated to be 0.62.

Chronoamperometric study

Chronoamperometry experiment was employed for evaluation of the diffusion coefficient of 4-NP at the modified electrode. According to the Cottrell equation [39]:

$$I = nFAD^{1/2}C\pi^{-1/2}t^{-1/2} \quad (5)$$

where n refers to the number of electron transferred ($n = 4$ for 4-NP [24]), F is the Faraday constant (96,485 C mol^{-1}), A is the effective surface area (0.047 cm^2), D is diffusion coefficient (cm^2 s^{-1}), C is the bulk concentration (mol cm^{-3}). Chronoamperograms were recorded by setting the working electrode potential at −920 mV for the Ni–Co_{OX} NP-modified GCE in the presence of various concentrations of 4-NP (Fig. 8). Figure 8a represents the experimental plots (I vs. $t^{-0.5}$) for different 4-NP concentrations employed. Afterwards, the slopes of these straight lines were plotted against the concentration

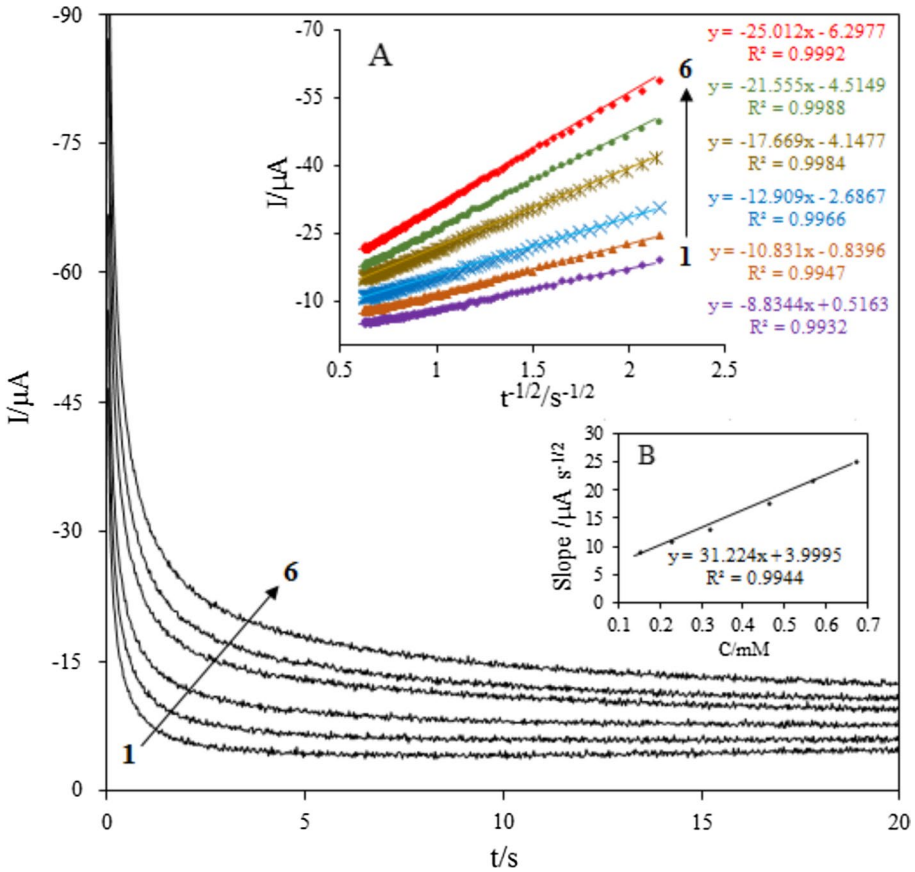

Fig. 8 Chronoamperograms obtained at Ni–Co_{OX} NPs/GCE in 0.1 M PBS (pH 6.0) for various concentrations of 4-NP. Numbers 1 to 6 correspond to 0.138, 0.215, 0.310, 0.449, 0.557, and 0.663 mM of 4-NP, respectively. *Insets a* Plots of I versus $t^{-1/2}$ and *b* Plot of the slope of the straight lines versus 4-NP concentrations

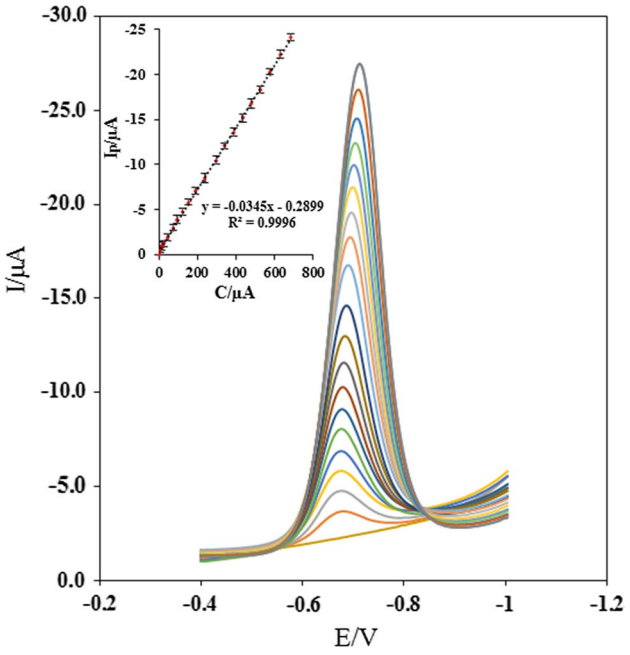

Fig. 9 DPVs for increasing concentrations of 4-NP from 7 to 682 μM in 0.1 M PBS (pH 6.0) on the Ni–Co_{OX} NPs/GCE at 50 mV s^{-1}. *Inset* Linear calibration plot (peak currents vs. 4-NP concentrations)

of 4-NP (Fig. 8b), and from the obtained slope and Cottrell equation, D was found to be 9.30×10^{-6} cm^2 s^{-1} [40–42].

Differential pulse voltammetry method and calibration curve of 4-NP

The differential pulse voltammetry method was employed to draw the calibration graph and determine the detection limit. As shown in Fig. 9, the reduction peak current increased linearly with the 4-NP concentration over the range of 7–682 μM in 0.1 M phosphate buffer solution, and the corresponding regression equation was I_{pc} (μA) = −0.0345 C (μM) − 0.2899. There was a minor shift for Ep with increasing the 4-NP concentration; this may be the limitation of the redox sites of Ni–Co_{OX} NPs and 4-NP in high 4-NP concentrations. The data for calibration curve were repeated three times. The detection limit for 4-NP with a signal-to-noise ratio (S/N) of 3 was calculated to be 4.8 μM. The comparison of proposed sensor with the previously reported sensors for determination of 4-NP is summarized in Table 1. As it can be seen, the proposed sensor exhibited wide linear range and reasonable detection limit.

Table 1 Comparison of the performance of the proposed sensor with previously reported electrochemical sensors for 4-NP

Electrode	Method	Linear range	Detection limit	Correlation coefficient	References
SWNT[a]/GCE	DPV	0.01–5.0	0.0025	_	[1]
Crown ether-Ag NPs/CPE[b]	DPV	1–100	0.25	_	[43]
S-CHIT/ABPE[c]	Derivative voltammetry	0.08–2	0.03	0.9996	[3]
Graphene–Nafion/SPE[d]	DPV	25–620	3.5	0.987	[44]
Nano-Au/GCE	LSV[e]	10–1000	8	_	[45]
GR-PANI[f]/GCE	DPV	0.2–20, 20–100	0.065	0.9930, 0.9987	[46]
PCZ/N-GE[g]/GCE	CV	0.8–20	0.062	0.9971	[47]
inorganic–organic/Pt	SWV[h]	30–90	8.23	0.9954	[48]
PDDA-G[i]/GCE	LSV	0.06–2, 10–110	0.02	0. 9964, 0.9977	[14]
ERG[j]-AuNP/GCE	LSV	0.036–90	0.01	0.9983	[4]
AC[k]/GCE	LSV	1–500	0.16	0.9863	[7]
Ni–Co_{OX} NPs/GCE	DPV	7–682	4.8	0.9996	This work

[a] Single-wall carbon nanotubes
[b] Carbon-paste electrode
[c] Acetylene black paste electrode coated with salicylaldehyde-modified chitosan
[d] Screen-printed electrode
[e] Linear sweep voltammetry
[f] Graphene–polyaniline
[g] Polycarbazole-/nitrogen-doped graphene
[h] Square-wave voltammetry
[i] Polyelectrolyte-functionalized graphene
[j] Electrochemically reduced graphene oxide
[k] Activated carbon

Table 2 Results for determination of 4-NP in practical samples

Sample	Added (μM)	Found[a] (μM)	RSD (%)	Recovery (%)
Spring water	20.00	20.54	2.34	102.70
	40.00	39.87	1.45	99.67
Tap water	20.00	20.58	2.04	102.90
	40.00	40.37	1.31	100.92

[a] Average of three determinations

Interference studies

The selectivity of the proposed sensor for the determination of 4-NP was studied by DPV technique under the optimum conditions with 0.1 mM 4-NP at pH 6.0. The tolerance limit for interfering species was described as the molar ratio of the interfering substance/4-NP, which caused a relative error of less than ±5% in the determination of 0.1 mM 4-NP. The results showed that 500-fold of Cl^-, Br^-, NO_3^- and 100-fold of Mg^{2+}, Ca^{2+}, Ni^{2+}, Co^{2+} did not show interference in the determination of 4-NP. However, the nitrophenols, such as 2-nitrophenol, 3-nitrophenol, and 2,4-dinitrophenol, were caused serious interference for the voltammetric signal of 4-NP because they included the nitro groups that could be reduced near the potential of 4-NP.

Analytical application

The practical performance of the proposed sensor was verified by the determination of 4-NP in environmental water samples such as tap water and spring water. No 4-NP was detected in these water samples, which may be ascribed to that the concentration of 4-NP was below for the detection limit. Thus, the water samples were spiked with known quantities of 4-NP, and the standard addition method was applied for the determination of 4-NP concentrations. As listed in Table 2, the recoveries were ranged from 99.67 to 102.90% with the relative standard deviations (RSDs) lower than 2.34% for 4-NP determination in all samples. It can be concluded that the proposed DPV method was reliable and could be successfully used for the detection of 4-NP in water samples. Furthermore, the interferences in water samples were almost negligible.

Conclusions

In this paper, a sensor based on Ni–Co_{OX} NP-modified GCE was constructed electrochemically by a two-step method for the detection of 4-NP. The modified GCE was characterized by SEM, EDX techniques. The SEM images showed the cauliflower-like nanoparticles with high density were distributed uniformly on the electrode surface. The EDX patterns also confirmed the presence of the Ni and Co nanoparticles on the electrode surface. The fabricated electrode showed significant electrocatalytic activity in the electroreduction of 4-NP. Some kinetic parameters (such as the diffusion coefficient, charge transfer coefficient, and the number of electrons involved in the rate-determining step) were estimated utilizing cyclic voltammetry and chronoamperometry techniques. A good linear range and reasonable detection limit were obtained using DPV experiments. Finally, the proposed electrochemical sensor was successfully used for the determination of 4-NP in environmental water samples. The electrochemical impedance spectroscopy (EIS) can be used as an electrochemical technique to characterize the surface of Ni–Co_{OX} NPs/GCE in the future researches.

Acknowledgements The authors are grateful to the research office of Tabriz University for the financial support.

References

1. C. Yang, Microchim. Acta **148**, 87 (2004)
2. R.M. de Oliveira, N.G. Santos, L. de Almeida Alves, K.C.M.S. Lima, L.T. Kubota, F.S. Damos, RdCS Luz, Sens. Actuators, B **221**, 740 (2015)
3. P. Deng, Z. Xu, Y. Feng, J. Li, Sens. Actuators, B **168**, 381 (2012)
4. X.X. Jiao, H.Q. Luo, N.B. Li, J. Electroanal. Chem. **691**, 83 (2013)
5. Y. Tang, R. Huang, C. Liu, S. Yang, Z. Lu, S. Luo, Anal. Methods **5**, 5508 (2013)
6. N.I. Ikhsan, P. Rameshkumar, N.M. Huang, Electrochim. Acta **192**, 392 (2016)
7. R. Madhu, C. Karuppiah, S.-M. Chen, P. Veerakumar, S.-B. Liu, Anal. Methods **6**, 5274 (2014)
8. D. Hofmann, F. Hartmann, H. Herrmann, Anal. Bioanal. Chem. **391**, 161 (2008)
9. M.I. Toral, A. Beattie, C. Santibañez, P. Richter, Environ. Monit. Assess. **76**, 263 (2002)
10. X. Guo, Z. Wang, S. Zhou, Talanta **64**, 135 (2004)
11. W. Zhang, C.R. Wilson, N.D. Danielson, Talanta **74**, 1400 (2008)
12. W. Huang, C. Yang, S. Zhang, Anal. Bioanal. Chem. **375**, 703 (2003)
13. Y. Zeng, Y. Zhou, T. Zhou, G. Shi, Electrochim. Acta **130**, 504 (2014)
14. D. Peng, J. Zhang, D. Qin, J. Chen, D. Shan, X. Lu, J. Electroanal. Chem. **734**, 1 (2014)
15. Z. Yin, S. Wu, X. Zhou, X. Huang, Q. Zhang, F. Boey, H. Zhang, Small **6**, 307 (2010)
16. Y. Ding, Y. Wang, L. Su, M. Bellagamba, H. Zhang, Y. Lei, Biosens. Bioelectron. **26**, 542 (2010)
17. W.-Z. Le, Y.-Q. Liu, Sens. Actuators, B **141**, 147 (2009)
18. M.-S. Wu, Y.-A. Huang, J.-J. Jow, W.-D. Yang, C.-Y. Hsieh, H.-M. Tsai, Int. J. Hydrog Energy **33**, 2921 (2008)
19. X. Kang, Z. Mai, X. Zou, P. Cai, J. Mo, Anal. Biochem. **363**, 143 (2007)

20. T. You, O. Niwa, Z. Chen, K. Hayashi, M. Tomita, S. Hirono, Anal. Chem. **75**, 5191 (2003)
21. B. Habibi, N. Delnavaz, RSC Adv. **6**, 31797 (2016)
22. M. Asgari, M.G. Maragheh, R. Davarkhah, E. Lohrasbi, A.N. Golikand, Electrochim. Acta **59**, 284 (2012)
23. M. Giovanni, A. Ambrosi, M. Pumera, Chem. Asian J. **7**, 702 (2012)
24. A. Noorbakhsh, M.M. Mirkalaei, M.H. Yousefi, S. Manochehri, Electroanalysis **26**, 2716 (2014)
25. Y. Zhang, Y. Wang, J. Jia, J. Wang, Sens. Actuators, B **171**, 580 (2012)
26. P. Cox, D. Pletcher, J. Appl. Electrochem. **20**, 549 (1990)
27. L. Tian, J. Bian, B. Wang, Y. Qi, Electrochim. Acta **55**, 3083 (2010)
28. A. Arvinte, F. Doroftei, M. Pinteala, J. Appl. Electrochem. **46**, 425 (2016)
29. L. Wang, X. Lu, Y. Ye, L. Sun, Y. Song, Electrochim. Acta **114**, 484 (2013)
30. M. Gu, Electrochim. Acta **52**, 4443 (2007)
31. A. Soto, E. Arce, M. Palomar-Pardave, I. Gonzalez, Electrochim. Acta **41**, 2647 (1996)
32. M. Gu, S.-B. Yao, S.-M. Zhou, Trans. IMF **84**, 196 (2006)
33. B. Singh, F. Laffir, C. Dickinson, T. McCormac, E. Dempsey, Electroanalysis **23**, 79 (2011)
34. M. Li, S. Xu, Y. Zhu, P. Yang, L. Wang, P.K. Chu, J. Alloys Compd. **589**, 364 (2014)
35. X. Wang, A. Sumboja, M. Lin, J. Yan, P.S. Lee, Nanoscale **4**, 7266 (2012)
36. M. Ranjani, Y. Sathishkumar, Y.S. Lee, D.J. Yoo, A.R. Kim, RSC Adv. **5**, 57804 (2015)
37. Y.-Y. Liang, S.-J. Bao, H.-L. Li, J. Solid State Electrochem. **11**, 571 (2007)
38. V. Gupta, S. Gupta, N. Miura, J. Power Sources **189**, 1292 (2009)
39. A.J. Bard, L.R. Faulkner, *Electrochemical Methods*, 2nd edn. (Wiley, New York, 2001)
40. R. Niesner, A. Heintz, J. Chem. Eng. Data **45**, 1121 (2000)
41. RdCS Luz, F.S. Damos, A.B. de Oliveira, J. Beck, L.T. Kubota, Talanta **64**, 935 (2004)
42. W. Liu, C. Li, Y. Gu, L. Tang, Z. Zhang, M. Yang, Electroanalysis **25**, 2367 (2013)
43. G. Rounaghi, H. Azizi-toupkanloo, Mater. Sci. Eng., C **32**, 172 (2012)
44. A. Arvinte, M. Mahosenaho, M. Pinteala, A.-M. Sesay, V. Virtanen, Microchim. Acta **174**, 337 (2011)
45. L. Chu, L. Han, X. Zhang, J. Appl. Electrochem. **41**, 687 (2011)
46. Y. Fan, J.-H. Liu, C.-P. Yang, M. Yu, P. Liu, Sens. Actuators, B **157**, 669 (2011)
47. Y. Zhang, L. Wu, W. Lei, X. Xia, M. Xia, Q. Hao, Electrochim. Acta **146**, 568 (2014)
48. S. Lupu, C. Lete, M. Marin, N. Totir, P.C. Balaure, Electrochim. Acta **54**, 1932 (2009)